PROCEEDINGS B

rspb.royalsocietypublishing.org

Research

Cite this article: Westermeier AS, Sachse R, Poppinga S, Vögele P, Adamec L, Speck T, Bischoff M. 2018 How the carnivorous waterwheel plant (*Aldrovanda vesiculosa*) snaps. *Proc. R. Soc. B* **285**: 20180012. http://dx.doi.org/10.1098/rspb.2018.0012

Received: 3 January 2018
Accepted: 13 April 2018

Subject Category:
Morphology and biomechanics

Subject Areas:
biomechanics, plant science

Keywords:
Aldrovanda, *Dionaea*, finite-element model, plant movement, reverse biomimetics, mechanical modelling

Authors for correspondence:
Anna S. Westermeier
e-mail: anna.westermeier@biologie.uni-freiburg.de
Renate Sachse
e-mail: sachse@ibb.uni-stuttgart.de

†These authors contributed equally to this work.

Electronic supplementary material is available online at https://doi.org/10.6084/m9.figshare.c.4079963.

THE ROYAL SOCIETY PUBLISHING

How the carnivorous waterwheel plant (*Aldrovanda vesiculosa*) snaps

Anna S. Westermeier[1,2,†], Renate Sachse[3†], Simon Poppinga[1,4], Philipp Vögele[1], Lubomir Adamec[5], Thomas Speck[1,2,4] and Manfred Bischoff[3]

[1]Plant Biomechanics Group and Botanic Garden (PBG), University of Freiburg, Schänzlestraße 1, 79104 Freiburg, Germany
[2]Freiburg Center for Interactive Materials and Bioinspired Technologies (FIT), Georges-Koehler-Allee 105, 79110 Freiburg im Breisgau, Germany
[3]Institute for Structural Mechanics (IBB), University of Stuttgart, Pfaffenwaldring 7, 70550 Stuttgart, Germany
[4]Freiburg Materials Research Center (FMF), University of Freiburg, 79104 Freiburg, Germany
[5]Institute of Botany of the Czech Academy of Sciences, Dukelská 135, 379 82 Třeboň, Czech Republic

ASW, 0000-0001-9281-1254; RS, 0000-0001-8895-9635; SP, 0000-0001-5341-9188; MB, 0000-0003-1538-4281

The fast motion of the snap-traps of the terrestrial Venus flytrap (*Dionaea muscipula*) have been intensively studied, in contrast to the tenfold faster underwater snap-traps of its phylogenetic sister, the waterwheel plant (*Aldrovanda vesiculosa*). Based on biomechanical and functional–morphological analyses and on a reverse biomimetic approach via mechanical modelling and computer simulations, we identify a combination of hydraulic turgor change and the release of prestress stored in the trap as essential for actuation. Our study is the first to identify and analyse in detail the motion principle of *Aldrovanda*, which not only leads to a deepened understanding of fast plant movements in general, but also contributes to the question of how snap-traps may have evolved and also allows for the development of novel biomimetic compliant mechanisms.

1. Introduction

Venus flytrap snap-trap physiology and mechanics are well understood [1], in contrast to those of the waterwheel plant (*Aldrovanda vesiculosa* L., Droseraceae). Aquatic *Aldrovanda* possesses free-floating, 10–30 cm long, rootless linear shoots with numerous leaf whorls of five to nine traps (figure 1*a*,*b*) and is the phylogenetic sister to the only other carnivorous plant with snap-traps, the terrestrial Venus flytrap (*Dionaea muscipula*) [2]. In both species, the traps are modified leaves consisting of two lobes connected via a midrib (figure 1*c*). Triggering of sensitive hairs (e.g. by touch) leads to trap closure. *Dionaea* possesses approximately 20 mm long aerial traps which typically close within 100–300 ms [3,4], whereas *Aldrovanda* develops 2–4 mm long underwater traps which shut within approximately 20–100 ms [5,6]. Two regions can be distinguished within each lobe [5] (figure 1*d*): (i) the three-layered central region comprises a parenchymatous middle layer surrounded by epidermis with elongated cells oriented perpendicularly to the midrib. It also incorporates the motor zone responsible for turgor change-based motion and numerous trigger hairs. (ii) The marginal, more flexible one-layered region consists only of epidermal cells.

Dionaea trap shutting relies on a combination of a turgor change-based slow movement, and a second, fast release of stored elastic energy by a sudden geometric change of its trap lobes (snap-buckling). The trap lobes of *Aldrovanda*, however, do not change curvature during trap closure (electronic supplementary material, video S1). Upon triggering, the turgor of inner-lobe epidermal cells located close to the midrib (motor zone) rapidly decreases due to potassium fluxes [7]. Consequently, the outer epidermal cells elongate, mediating midrib deformation from a straight into a bent configuration and trap closure

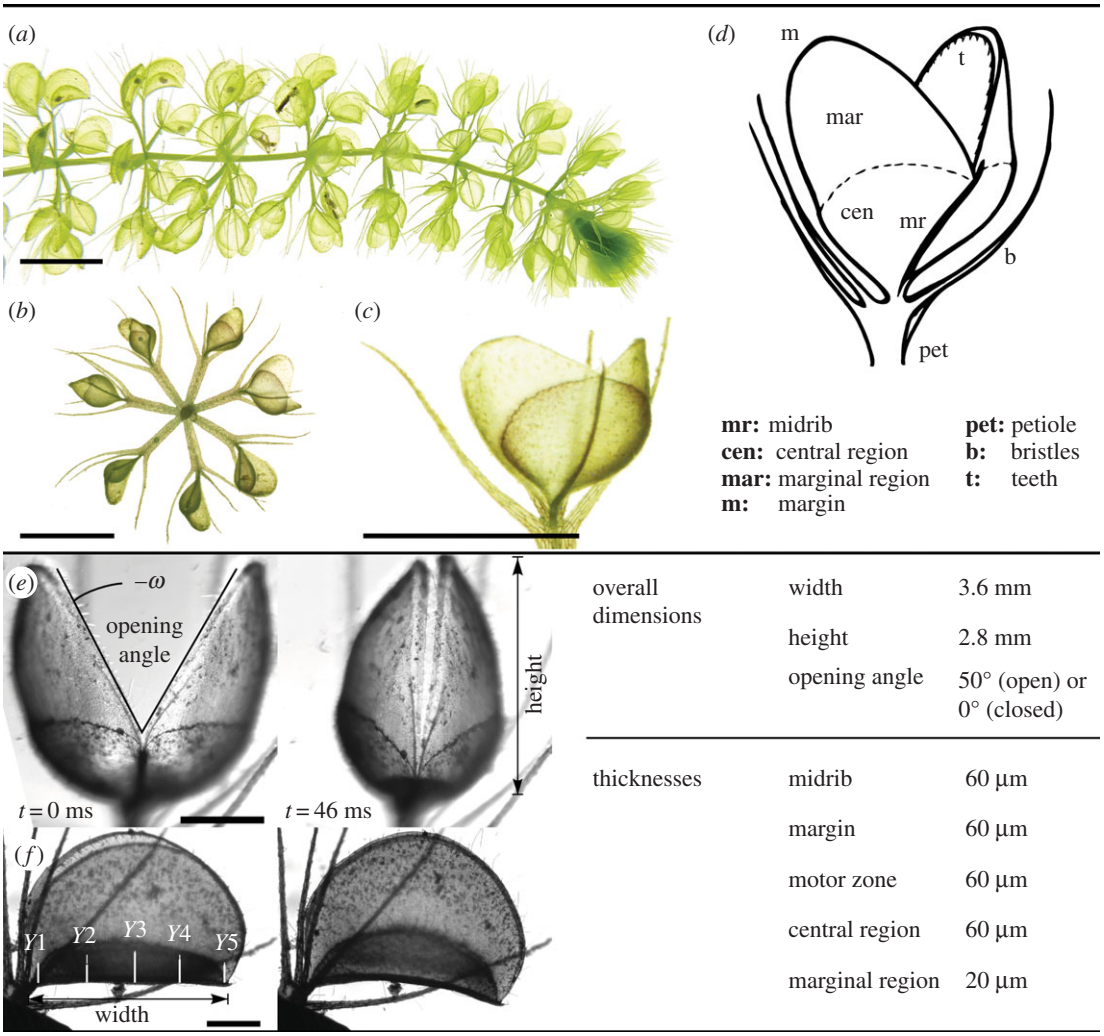

overall dimensions	width	3.6 mm
	height	2.8 mm
	opening angle	50° (open) or 0° (closed)
thicknesses	midrib	60 µm
	margin	60 µm
	motor zone	60 µm
	central region	60 µm
	marginal region	20 µm

Figure 1. Vegetative morphology of *A. vesiculosa*, shutting of a trap (temperate ecotype TempE, at 13°C water temperature) and morphometric parameters for FE models based on values measured in an exemplary specimen (TempE). (*a*) Lateral view on a free-floating shoot with numerous traps (TempE). (*b*) Frontal view on a whorl with open and closed traps (tropical ecotype TropE). (*c*) Single, open trap. (*d*) Schematic drawing of an open trap with the regions and other morphological features highlighted. Scale bars, (*a–c*) 1 cm. (*e*) Apical view, opening angle and measured angular velocity ω indicated. (*f*) Lateral view (same trap as *e*), the midrib deformation measurement points *Y1–Y5* are indicated (see Material and methods). Scale bars, (*e,f*) 1 mm.

(figure 1*e,f*). Owing to kinematic coupling to the midrib, the lobes are 'enforced' to move towards each other [6].

According to Cameron *et al*. [2], *Aldrovanda* and *Dionaea* share an unknown common ancestor. Although the two species apparently employ different motion principles, hypotheses regarding snap-trap evolution have focused only on the influence of prey size on trap sizes using qualitative models [8,9] but not on other selective factors such as movement mechanics and possible adaptations to the different habitats.

There exist no detailed kinematic and functional-morphological analyses of the *Aldrovanda* trap until now. The kinematic amplification mechanism [6] is based only on a single trap recording from which also the hypothesis that the midrib might be pretensioned was derived and which also lacks corroborating analyses of the midrib bending and trap closure interrelation, functional–morphological investigations on real traps, as well as a model on potential prestress. Hence, the actuation principle is unclear because *Aldrovanda* can be found at the transition between plant movements empowered by elastic instabilities and hydraulics [10]. We performed detailed biomechanical and functional-morphological analyses in combination with mechanical models and finite-element (FE) simulations and discuss our findings regarding snap-trap evolution.

2. Material and methods

(a) Plant material

Plant material of two *Aldrovanda vesiculosa* ecotypes was provided by L.A. from the collection in the Institute of Botany of the Czech Academy of Sciences at Třeboň, Czech Republic, and cultivated in the Botanic Gardens Freiburg (according to Adamec [11,12]). Two ecotypes were investigated [13]: (i) a tropical ecotype (TropE) initially collected from Girraween Lagoon, approximately 30 km southwest of Darwin, NT, Australia, which was grown in aquaria in the tropical greenhouse and (ii) a temperate Central-European ecotype (TempE) initially collected from Lake Długie, Łezna-Włodawa Lake District, East Poland, which was grown outside in a water tank.

(b) Kinematics: stereo high-speed camera set-up

A MotionScope Pro Y4 high-speed camera (IDT, Inc., USA) was mounted on a SZX9 stereo microscope (Olympus, Japan) for recording trap motion from apical view, and complementary,

for lateral recordings, a NX4-S1 high-speed camera (IDT, Inc., USA) mounted on a Wild M420 stereo microscope (Wild Heerbrugg, Switzerland). The cameras were synchronized using the software Motion Studio (v. 2.12.16, IDT, Inc., USA). Two cold light sources were employed (Endoscope techno light 270, Karl Storz GmbH & Co. KG, Tuttlingen, Germany, and Constellation 120 high-performance LED light source, IDT Inc., USA). To trigger the traps electrically, the set-up by Ashida [5] was adapted. Two aluminium plates (electrodes) were connected to a power supply (Programmable DC Power Supply DP832, Rigol, China) and the electrical triggering impulse was set to 30 V (according to Ashida [5]: less potential does not guarantee trap closure, more potential enforces 'narrowing movement'). The electrodes were placed into an aquarium (volume approx. 2.5 l) filled with artificial pond water (APW: KNO_3 0.1 mM, $NaHCO_3$ 0.20 mM, $CaCl_2$ 0.25 mM, $MgSO_4$ 0.10 mM). Dissected, open traps (with the midribs facing the cathode, cf. [5], were then carefully positioned between the plates using ceramic tweezers (Carl Roth Inc., Germany). All traps were of the same age (mature whorl 7 seen from the plant apex, different individuals) (cf. [14]). Used traps were around 3–4 mm long. The water temperature was kept at 23°C or 13°C. The recording speed was set to 1000 fps, with $n = 20$ (traps) for each trial (each ecotype at each temperature regime).

(c) Water displacement

For qualitative visualization of water flows during snapping, tracer particles (hollow glass spheres, diameter 2–20 µm, $p = 1.1$ g cm^{-3}) (Polysciences Inc., Washington) were carefully added to the water and the traps triggered using a thin Nylon thread. Recording was performed using the aforementioned equipment.

(d) Kinematical analyses

The high-speed recordings were processed using Fiji v. 2.0.0 [15]. First, the trap lobe motion was analysed from apical view by measurement of the change of angle between the two lobes (figure 1*e*) and the maximal angular velocity ω calculated. To compare the $n = 20$ recordings, the duration of the quick shutting phase (QSP) was defined as double the time from movement beginning until the maximum angular velocity was reached (see Results). Durations for each trial were checked for normal distribution with Shapiro–Wilk's test. The trials were then statistically compared to each other by a Welch two-sample *t*-test with $p < 0.05$ taken as significance level by using the R software v. 3.2.4 [16]. In order to quantify the midrib deformation from lateral view, from each trial single frames from five randomly chosen high-speed recordings were manually aligned using Photoshop CS5 v. 12.0 × 64 (Adobe Systems Software Ltd, Ireland). The connection between the basal and apical insertion points of the lobes to the midrib was taken as baseline. Each baseline was divided into four equal parts, resulting in five defined points on the midrib referred to as *Y*1–*Y*5, with *Y*3 representing the central point on the midrib (figure 1*f*). The ratios between trap lobe length at the vertex points of *Y*1–*Y*5 and midrib length were calculated and the resulting ratios taken to normalize the displacement of *Y*1–*Y*5 for each trap. By this, the proportion of the *Y*-displacement in relation to the midrib could be evaluated. The displacement of each of the defined positions relative to the midrib length was measured. Shortening of the midrib in the *X*-direction during the bending could not be discriminated from the error of measurement and was subsequently excluded from analyses. Correlation between trap opening angles and shutting durations was calculated according to Spearman's test (rho, non-normally distributed data) using R (negative correlations: correlation coefficient less than −0.3, positive correlations: greater than 0.3).

(e) Functional morphology: light microscopy

Fresh plants were fixed in FAA fixation and entire whorls embedded in Technovit resin. Single traps were thin sectioned (5 µm) using a custom-made rotary microtome. Sections were examined with a BX61 light microscope equipped with a DP71 digital camera and cell'P v. 2.6 software (Olympus, Tokyo, Japan)

(f) Scanning electron microscopy

Single traps were dehydrated according to Neinhuis & Edelmann [17], critical-point dried (Critical Point Dryer Bal-Tec CPD030, Switzerland), gold-sputtered (Cressington Sputter Coater 108 auto, Germany) and mounted on aluminium stubs with conductive pads. A scanning electron microscopy (SEM) 435VP was used (LEO Electron Microscopy, England).

(g) Manipulative experiments

Razorblade cuttings were applied to different regions of closed traps lying in a droplet of water. Different areas were cut (for each: $n = 5$–10) and the resulting deformation observed using a stereomicroscope and PixeLINK USB 3.0 camera with the µScope software v. 20.1 × 64 (PixeLINK, Ottawa, Canada).

(h) Simulation

The simulations are based on FE models calculated with a geometrically nonlinear static analysis using ANSYS (release 18.0, ANSYS Inc., Canonsburg, USA). Hydromechanical effects from the surrounding water were neglected. As the overall load displacement path is stable—as opposed to the Venus flytrap's one—there is no 'self-acceleration' due to instabilities (snap-through). Consequently, in the theoretical limit of a quasi-static actuation, there are no inertia effects or damping in *Aldrovanda* and were as such neglected in the FE models. The trap tissue material was idealized and assumed to have an isotropic and linear elastic behaviour with a Young's modulus of $E = 10$ MPa (typical values for plant parenchyma: 0.3–14 MPa [18]) and a Poisson's ratio of $\nu = 0.3$. Owing to (i) the occurrence of a central vascular bundle that consists of more and smaller cells and (ii) its orthogonal cell orientation, we assumed a higher Young's modulus of the midrib ($E = 30$ MPa). A short parameter study regarding the stiffness ratio was conducted for model 3 (electronic supplementary material, text S1 and figure S1). For qualitative analysis of deformation behaviour and stress distribution, only the stiffness ratio between the different regions is crucial. As the material model is simple and the related parameters are not accurately known, it neglects the complexity of the biological tissue. For this reason, no quantitative values for stresses could be evaluated, but the given values allow for a good first-order estimation. For the description of the geometry, different element types were used. Linear components were modelled with shear deformable Timoshenko beam elements, which allow for normal forces as well as bending and shear. They were discretized by two-node linear elements (BEAM188). Owing to the small thickness of the lobes, shell assumptions apply for two-dimensional regions. A shear deformable Reissner–Mindlin shell model was used and discretized by four-node quadrilateral elements (SHELL181). The trap morphometry used in the computer models was based on measurements of an exemplary specimen and remained consistent in all models (figure 1). As traps show a typical opening angle of 50° (electronic supplementary material, table S1), this was taken as the target value (slightly less than in the exemplary specimen). To first analyse single effects of the trap motion and afterwards a combination of all observed effects, three models with increasing geometrical and mechanical complexity were constructed (electronic supplementary material, figure S2).

(i) Model 1: analysis of kinematic behaviour of the trap

Model 1 served to simulate the basic kinematic behaviour of the trap when the midrib is bent. It is an approximation of the geometry with linear beam elements, where the sum of the cross-sectional areas is equivalent to the actual cross-sectional area of the lobe. As the focus is on the deformation and bending of the midrib, the displacement constraints are those of a single-span beam. In order to investigate coupling between bending of the midrib and closure of the trap, two different load cases were applied: a distributed vertical load on the midrib (0.125 N mm^{-1}) and a longitudinal contraction due to a temperature load with a thermal coefficient of 1, mimicking turgor change (volume expansion/contraction), but not experimental (electronic supplementary material, figure S3A).

(j) Model 2: analysis of prestress within the trap

For a more detailed investigation of the prestress distribution throughout the central region in the closed trap, the real geometry was better approximated by including more elements (BEAM188). The refined geometry is able to represent the lobe curvature more accurately (electronic supplementary material, figure S2). As an experimental investigation of the prestress state in the highly sensitive open trap is not possible, a simulation was performed to deduce this prestress situation from the derived state of the closed trap. More precisely, the open state is deduced via a backward simulation starting from the closed state. This state is assumed to be the relaxed state (no/less prestress) without any loads and represents, therefore, the initial model configuration. The application of loads (compressive stress on midrib) caused trap opening. A subsequent unloading would follow the same deformation process backwards for a quasi-static simulation in the given limits of simple elastostatic modelling, as the stable quasi-static process has a convex potential. To avoid rigid body motions, model 2 was constrained like a cantilever beam where all degrees of freedom, three translations and three rotations, were fixed at one side of the midrib, representing the connection to the petiole.

(k) Model 3: combined model of prestress and kinematics

Model 3 was used for (i) a verification of the prestress effects analysed by model 2, as well as for (ii) investigation of movement due to turgor change in the motor zone and (iii) for a combination of the aforementioned two load cases. In order to correctly model the mechanical behaviour of the lobe as a two-dimensional thin-walled structure, shell finite elements were used for the representation of the lobes. The midrib and the lobe margins are modelled by beam elements. As in model 2, the displacement constraints represent those of a cantilever beam and the closed state corresponds to the relaxed state. To simulate the effects of turgor decrease in the motor zone, three different load cases were applied. An increase in the temperature represents an increase in turgor, whereas a temperature decrease has the opposite effect. To investigate the effect of turgor change in the motor zone, first an isotropic temperature load was applied. Then—to include the influence of cell orientation as seen in the real trap (see Results)—the influences of an expansion perpendicular to the midrib and as well as of a parallel expansion were analysed. In each case, the value of expansion applied to the motor zone was adjusted to achieve an opening angle of targeted 50° as seen in real traps (figure 1; electronic supplementary material, table S1). For the final combined model 3, the perpendicular turgor load case and prestress on the midrib were brought together.

3. Results

(a) Kinematics

We define the QSP as twice the time until maximal lobe angular velocity ω is reached during trap closure (figure 2*a*). QSPs last 18–48 ms (median 28 ± 8) in temperate ecotype TempE and 26–96 ms (median 46 ± 20 ms) in tropical ecotype TropE at 13°C, and 14–26 ms (TempE, 20 ± 4 ms) and 16–30 ms (TropE, 22 ± 4 ms) at 23°C (figure 2*b*). A characteristic bell-shaped curve of ω can be observed in all recordings (figure 2*a*). By the end of the QSP, the traps possessed opening angles of 0°–5°.

Midrib bending deformation proceeds similarly in all recordings (electronic supplementary material, figure S4) with the strongest displacement of the central midrib point *Y*3 (figure 1*f*), especially at high temperature (electronic supplementary material, figure S5). The *Y*3 displacement and, therefore, the bending of the midrib proceeds quickly at the beginning until it plateaus (figure 2*c*). The progression of the opening angle follows the same temporal course. It decreases continuously during trap closure, at the end of the QSP, however, also at lower speed until it also plateaus (figure 2*d*). This plateau coincides with the declination of ω, confirming the angular velocity as time derivative of the opening angle, as well as the displacement. It can be seen that both processes proceed simultaneously and are thus coupled.

The duration of the QSP is independent of the initial opening angle (electronic supplementary material, table S1) (Spearman's correlation analysis, $\rho = -0.272$, $n = 88$). The QSP duration of TropE (median 46 ± 20 ms) and of TempE (median 28 ± 8 ms) at low temperature (13°C) are highly significantly different (Welch two-sample *t*-test, d.f. = 23.861, $p = 0.0001$), whereas no significant difference can be attributed to the QSP durations at high temperature (23°C) (TropE: 22 ± 4 ms; TempE; 20 ± 4 ms) (Welch two-sample *t*-test, d.f. = 38.99, $p = 0.13$) (figure 2). The QSPs also differ highly significantly for 13°C and 23°C within each ecotype (TempE: $t = 5.69$, d.f. = 33.396, $p < 0.00001$; TropE: $t = 6.5675$, d.f. = 20.371, $p < 0.00001$).

A change of trap lobe shape before and after closure is indiscernible from an error of measurement with the methods used herein.

Water beyond the central region becomes pushed out of the trap during shutting (electronic supplementary material, video S2). An investigation of the various load cases on a simplified FE model (model 1), which analyses the effect of midrib bending on the trap kinematic, is given in electronic supplementary material, text S2 and figure S3.

(b) Functional trap morphology

Distinct structural differences between the motor zone (thickness approx. 0.06 mm) and the other regions were not detected (figure 3*a*,*b*). The cells of the central region are elongated and oriented perpendicular to those of the midrib (figure 3*c*). In addition, many glands of unknown function can be observed abaxially and adaxially along the approximately 0.1 mm thick midrib.

(c) Prestress within the trap

Manipulation experiments (figure 4*a*–*d*) highlight tissue stress distributions within a closed trap, from which a

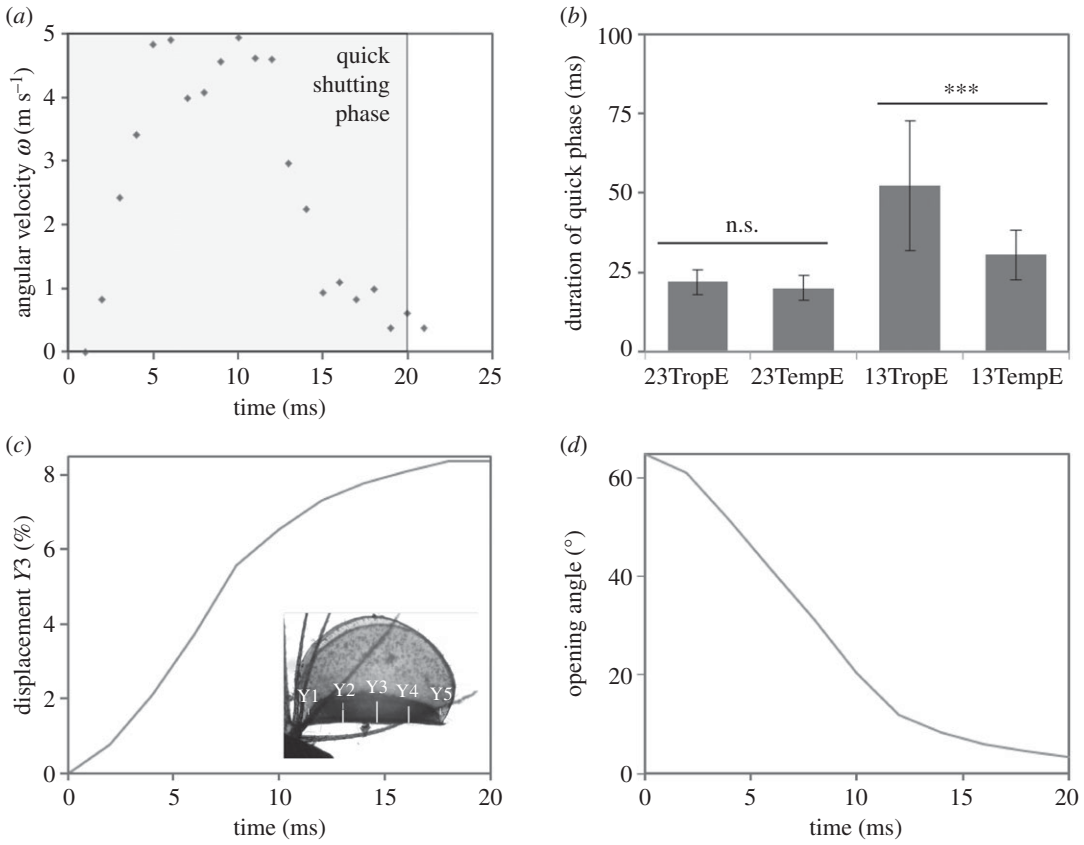

Figure 2. Comparative trap shutting analyses of the two ecotypes. (*a*) Display of the quick shutting phase (QSP) in an exemplary measurement (23°C TempE). (*b*) The shutting durations of the two ecotypes differ highly significantly at 13°C but not at 23°C. Within each ecotype the QSPs also differ significantly for 13°C resp. 23°C. (*c*) Displacement progression during closure until maximal displacement of the midrib centre in relation to the midrib length is reached. (*d*) Change of trap opening angle during closure.

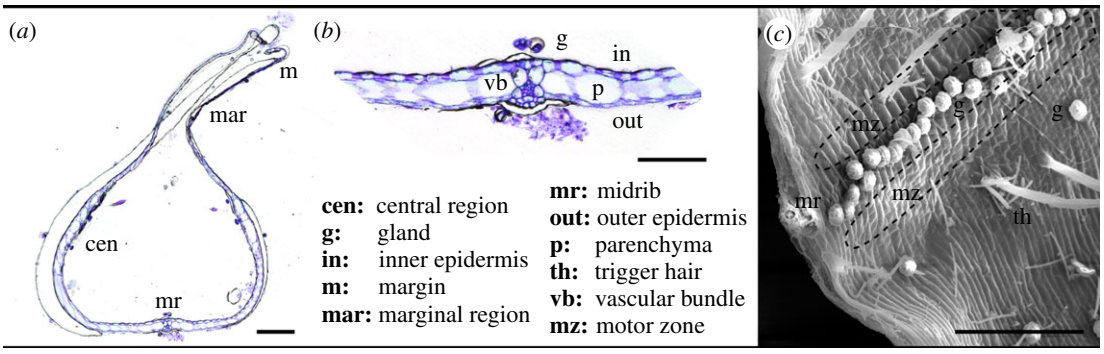

Figure 3. Functional trap morphology. (*a*) LM transversal section through a closed trap (in the very narrowed state *sensu* [5]). Scale bar, 200 µm. (*b*) LM detail of the midrib and adjacent regions. Scale bar, 100 µm. (*c*) SEM image of a transversally cut trap, location of motor zone highlighted (dashed lines). Scale bar, 200 µm.

possible equilibrium trap state can be derived (figure 4*e*,*f*). Gaping upon cutting indicates the release of tensile prestress. No gaping either indicates that no prestress is present or the release of compressive prestress.

Cutting into the marginal region of a closed trap and stopping before the central region does not indicate prestress (figure 4*a*). However, when the central region is reached, the cutting gapes (figure 4*a*). Cutting the midrib does not lead to gaping, but cutting the central region does (figure 4*b*). When separating the midrib from the rest of the trap, it relaxes into a strongly bent configuration (figure 4*c*). Cutting the central region parallel to one side of the midrib results in an inward curl of the lobes' tissue (figure 4*d*).

Therefore, tensile prestress in the central regions, compressive prestress in the midrib and no prestress in the marginal regions can be attributed to the closed trap. The state of equilibrium between tensile and compressive prestress is maintained at any location within the trap. Taking the midrib curvature and the cell orientation in the central region perpendicular to the midrib into account, equilibrium enforces a decrease of the tensile prestress magnitude parallel to the midrib from both directions (midrib end and base) towards the trap centre (figure 4*f*), indicated by the arrow sizes. The trap behaviour due to an application of prestress on the midrib was simulated with a further refined simplified FE model (model 2). A compressive prestress on the midrib mainly leads to tension in the central region. The trap tends to open and the midrib to straighten when the compressive prestress increases (electronic supplementary material, video S3). Although a simple superposition of different

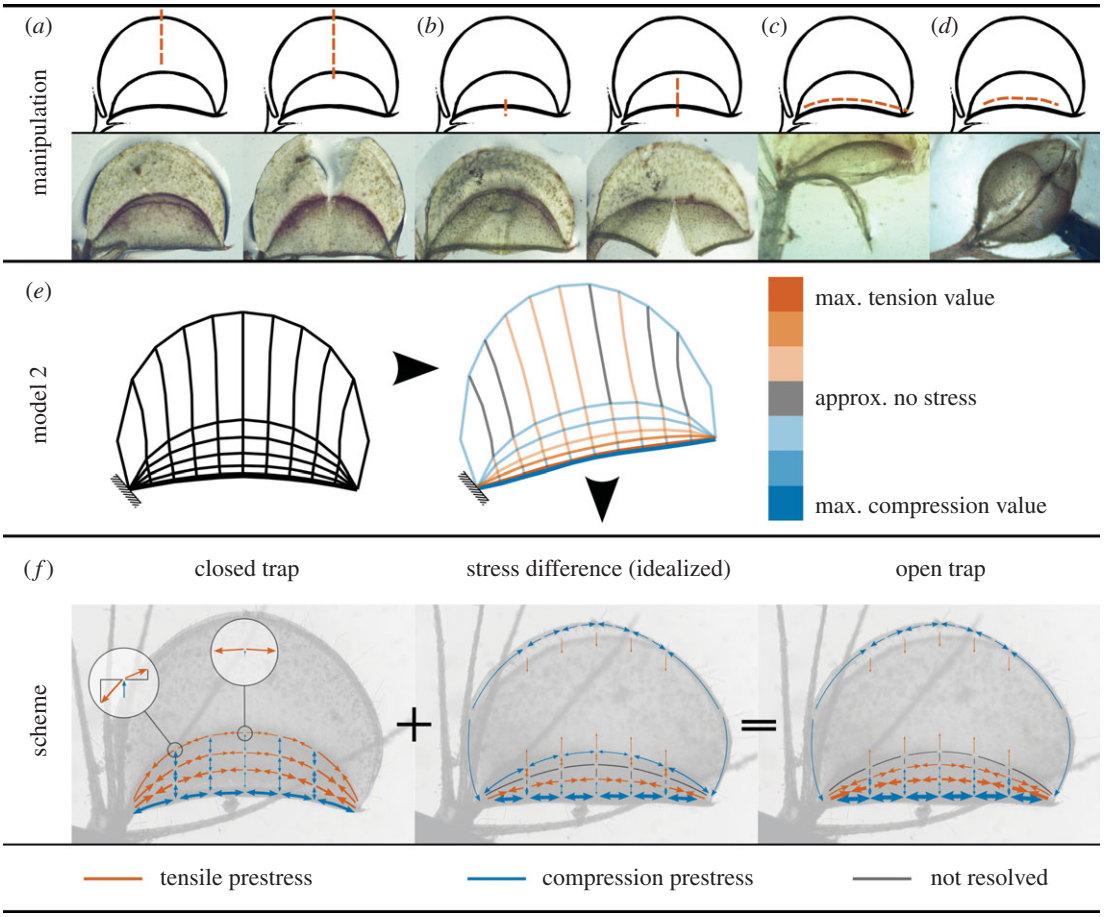

Figure 4. Prestress states of traps. (*a–d*) Manipulative experiments on closed traps with cut length and location and the resulting behaviour. (*e*) Simulation results of model 2 with an applied compression prestress on the midrib. (*f*) Assumed prestress state in the closed trap and prestress state of the open trap derived from stress difference.

load cases is not applicable in geometrically nonlinear analyses, the results indicate prestress differences between the closed and the open trap state. Therefore, a combination of the derived prestress state of the closed trap and the calculated difference gives an idea of a possible prestress situation in the open trap (figure 4*e*; electronic supplementary material, video S4). Owing to the assumptions and simplifications in the model, no quantitative values were obtained. For the same reason, it is not clear whether a tensile or compressive prestress dominates in the transition zone between the central and marginal region.

A turgor increase in the stiffer (compared to the other trap tissue) midrib and a subsequent elongation of the cells inside generate compression prestress as observed in the real trap. It results from the constraint on the turgor-induced deformation of the midrib imposed by the rest of the trap. Comparing both states, the midrib partly releases its compressive prestress during closure. This load case is equivalent to the applied temperature load case on model 1 and the resulting bending of the midrib because of its eccentric location (see electronic supplementary material, text S2 and video S5).

The application of the same prestress load case in model 2 and a detailed FE model (model 3) serves for verification if the results are equivalent. Without taking quantitative values into account, the results, especially the distribution of tension and compression stresses, are similar (electronic supplementary material, figure S6). The value of the applied compressive prestress to the midrib allows for an approximate straightening of the midrib and corresponds to an individual cell elongation of 2.4%. However, even when the midrib is straightened, an opening angle of only 22° (instead of the targeted 50°, figure 1) is reached.

(d) Influence of motor zone turgor changes on the trapping motion

The influence of turgor change in the motor zone was examined by application of different load cases to a backward simulation of model 3, where individual effects like directional turgor changes, can be isolated. First, an isotropic cellular expansion of the motor zone was investigated, followed by a separately modelled split of the two directions parallel and perpendicular to the midrib. Additionally, these three different load cases were applied either throughout the thickness, i.e. on the whole tissue or only on the inner epidermis, leading to six different load cases in total (figure 5).

An isotropic cellular expansion works well for trap closure/opening and also an adequate coupling between midrib deformation and lobe movement is observable. In contrast to this, only the turgor change in the inner epidermis of the motor zone leads to an increase of the midrib curvature which does not represent the natural situation (electronic supplementary material, video S6). Similar results are obtained from the load case of cellular deformation parallel to the midrib. By increasing the turgor only in the inner epidermis, the trap opens and then starts to reclose again (electronic supplementary material, video S7). Contraction

(*a*)

load case	load location	motor cell elongation	curvature change of midrib
 isotropic expansion	whole tissue	14%	decrease (approx. straight)
	inner epidermis	18%	increase
 expansion parallel to midrib	whole tissue	18%	decrease (approx. straight)
	inner epidermis	—	increase
 expansion perpendicular to midrib	whole tissue	50%	decrease (approx. straight)
	inner epidermis	19%	approx. no change

(*b*)

load case	prestress	turgor	turgor and prestress
		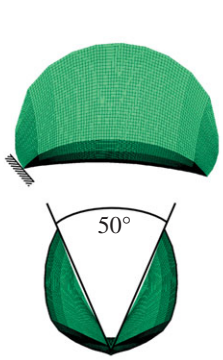	
max. cell elongation	2.4%	19%	6.5%

Figure 5. Different load cases of model 3. (*a*) Different load cases representing turgor changes within the motor zone for trap opening (opening angle target value: 50°), respective required motor cellular elongation and curvature change of midrib during deformation compared with the initial, closed configuration. (*b*) Resulting deformation, trap opening angle, midrib configuration and maximum motor cell elongation in the three different load cases (see electronic supplementary material, figure S1 and videos S7–S10).

of the inner epidermis perpendicular to the midrib, however, does not lead to any midrib curvature change. Even though, in this simulation, the trap is able to open up to the targeted 50° (figure 5, electronic supplementary material, video S8), the coupling of midrib deformation and lobe closure are not as distinct. This load case requires a motor cell elongation of 19% and represents the turgor change and according cell elongation/expansion behaviour most realistically (i.e. longitudinal cell elongation, [19], figure 5). It is, therefore, the basis for the following simulations and referred to as the turgor load case.

Eventually, the two working load cases (prestress effects and hydraulic actuation) are combined. The model that simulates trap opening solely due to prestress achieves a trap opening angle of 22° (electronic supplementary material, videos S3 and S4). The combination of volume changes in the motor zone and prestress results in an opening angle of 50°, an approximately straight midrib, and reduces the required motor cell elongation to 6.5% (figure 5; electronic supplementary material, video S9).

4. Discussion

Until now, the actuation of the *A. vesiculosa* trap was not entirely understood and thought to be purely hydraulic [10]. Based on our analyses, it can be confirmed that a small bending deformation of the midrib is accompanied by the closing of the two trap lobes (kinematic amplification) [6], and show for the first time that movement actuation is a combination of active hydraulics and the release of internal prestress. It was impossible for us to evaluate the individual temporal progressions and possible interrelations of the different actuating components, and we can only hypothesize that they run simultaneously. Our findings suggest defining the QSP as twice the time until ω_{max} is reached. In figure 2*a*, two peaks of ω can be observed, which is thought to be due to (i) minimal movement difference in consecutive frames and (ii) unrecognized tissue anomalies in the biological specimen itself. In other recordings, only one peak of ω can be observed (data not shown). The decrease of ω after ω_{max} may be explained by a water damping effect (WDE), which is caused by the evenly distributed displacement of fluid out of the trap during closure (electronic supplementary material, video S2). The WDE can also explain the bouncing of the traps during shutting (electronic supplementary material, video S1). Owing to the cantilever set-up of the trap, it moves downward when closing and the displaced water probably applies a reactive impulse. It must be noted that our assumptions are made on qualitative observations and we assume that the water has an influence on snapping speed but not on the mechanism itself because the trap lobes

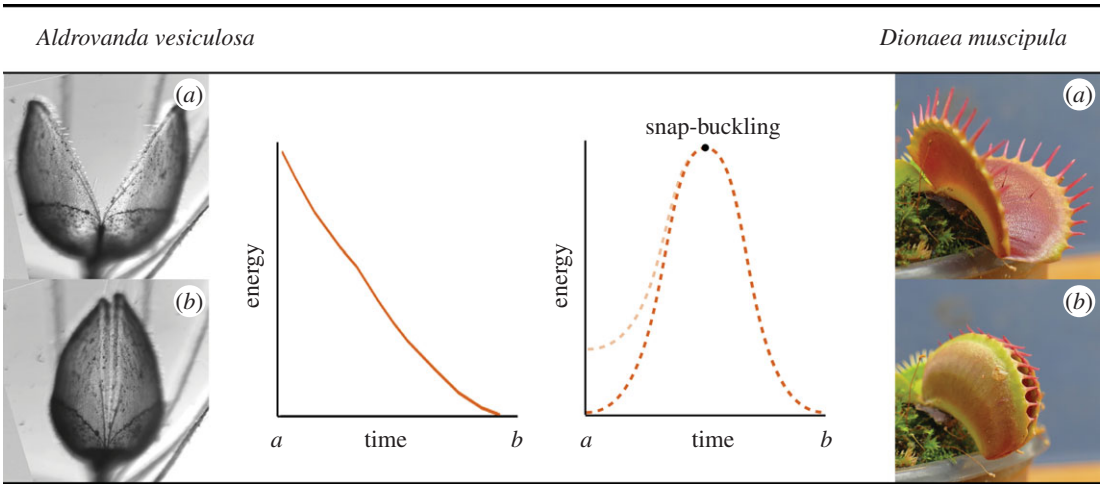

Figure 6. Elastic energetic states during closure in *Aldrovanda* and *Dionaea*. In *Aldrovanda*, the potential energy is smoothly released (derived from simulation). By contrast, *Dionaea* displays the conceptual characteristic energy curve for snap-buckling with the two stable states 'open' (*a*) and 'closed' (*b*), possessing the lowest E_{pot} [20].

do not change shape during shutting. Therefore, WDEs are also neglected in the simulations partly because of the complexity connected to fluid dynamics. The fluid body inside the trap up to the transition of the central to the marginal regions becomes 'entrapped' (electronic supplementary material, video S2). Potential prey triggers one of the numerous sensitive hairs at the trap bottom, thereby being within the 'fluid volume reach' of the trap, i.e. the prey will not be flushed out.

Trap closure durations of TempE and TropE were shown to be highly significantly different between cold (13°C) and warm (23°C) temperature regimes. Probably, these differences are adaptations to the individual habitats (temperate versus tropical), representing a striking example of microevolution. The temperature dependence of the snapping duration is also an indicator for the active hydraulic component of the trap movement relying on physiological processes.

The calculated poroelastic time *tp* approximately 0.004 s for *Aldrovanda* [10] is in agreement with our own measurements of motor zone thickness (approx. 60 µm) and closure durations (figures 2 and 3; electronic supplementary material, table S1). Theoretically, the trap may work purely hydraulically. Owing to the orientation of the motor cells perpendicular to the midrib (figure 4*c*), we may hypothesize that they elongate in the same direction during actuation, similarly as reported for Venus flytrap [3] and in accordance with cell expansion behaviour for elongated cells [19].

Model 3, which investigated the effect of hydraulic actuation of the motor zone with cellular elongation perpendicular to the midrib in the inner epidermis, resulted in the target value of 50° opening angle. This required a relatively large cell volume change of 19% (figure 5). It has also to be noted that, in this computer model, the midrib remained in a bent configuration (in contrast to the natural trap where the midrib becomes straight).

According to our simulations, there is an elaborate equilibrium between compressive prestress within the midrib and tensile prestress within the adjacent tissues of the central regions. The marginal regions are apparently excluded from this interplay by not being prestressed. The model simulating the trap motion solely relying on midrib prestress showed that opening angles greater than approximately 22° cannot be achieved, although the midrib changed from bent to straight (figure 5). Prestress is probably further released when the trap turns into the narrowed and very narrowed stages after the QSP [5], when the midrib is even further bent.

The combination of the two working load cases (hydraulics, prestress) in a backward simulation resulted in an open trap, which not only achieved a trap opening angle of 50° with a straight midrib, but also required only 6.5% of cell volume change in the motor zone. This is in very good agreement with *Dionaea* trap surface strain-field-analyses [3]. It also represents the efficacy of the *Aldrovanda* motion principle because less time is needed for such a volume change (compared to 19% as seen in model 3, perpendicular expansion of inner epidermis) required for actuation. Moreover, we hypothesize that the incorporated prestress not only diminishes the decreased coupling effect of midrib deformation and lobe closure, but that it also might act as speed boost, as explained in the following.

We assumed that water damping naturally increases the closing duration in traps with wide opening angles due to a greater fluid volume to be displaced. However, we did not find any such correlation according to the Spearman analysis. Therefore, it can be hypothesized that wider open traps may bear greater prestress due to storage of more elastic energy, which—as speed boost—would compensate the loss of speed by water resistance. It would be of interest for future investigations to check if juvenile *Aldrovanda* traps rely to a greater extent on hydraulics because of the more flexible tissue than older, more rigid traps ([5], A.S.W. 2017, personal observation), which might employ more prestress to achieve short trapping durations. The fact that less strain energy in the motor zone is required if prestress is present, will not be changed in the presence of (hydro-)dynamic effects, because the underlying actuation principles will probably comply with the actual behaviour.

Looking at the elastic energy release of *Aldrovanda* and *Dionaea* during closure, the difference between the two motion principles becomes especially striking. Figure 6 shows a comparison of the computed strain energy in *Aldrovanda* and a conceptual sketch of the strain energy in *Dionaea*. In *Dionaea*, the lobes rapidly invert their curvature when the geometric constraint induced by the double curvatures of the

lobes is overcome by snap-buckling, whereas in *Aldrovanda* the energy is smoothly released, without any sudden acceleration of the trap. This can be explained by the incorporated kinematic components. *Aldrovanda* trap employs hydraulics, elastic relaxation and kinematic amplification, whereas the Venus flytrap employs an initial hydraulic deformation, followed by elastic instability. The different mechanical principles for snapping are related to physical limits such as trap size and tissue thickness which both fundamentally differ in the two traps [10].

Full functionality (in terms of motion speed) of hydraulically actuated structures is ultimately limited by water flow processes within the tissues [21]. To overcome these limitations in terms of snapping duration, the large traps of *Dionaea* employ a snap-buckling instability [10]. The required, large geometric changes in overall trap shape linked to snap-buckling might be correlated with high energetic costs. Snap-buckling in *Aldrovanda* might, however, be disproportionate to its trap size and thus, probably overly energy-demanding and disadvantageous. Consequently, kinematic amplification would be a suitable way to achieve sufficiently fast and 'economic' plant motions for small structures. This is further confirmed by the fact that traps of juvenile *Dionaea*, which are similar in size to those of adult *Aldrovanda*, do not yet employ snap-buckling for closure but presumably move purely hydraulically, yet much slower than *Aldrovanda* traps [4]. As shown in this study, the faster snapping motion in *Aldrovanda* can, in turn, be explained by the speed boost due to the incorporated prestress.

Despite the close phylogenetic relationship between *Dionaea* and *Aldrovanda*, originating from a common unknown ancestor, it is still unclear why they evolved such diverging trap sizes with differing motion principles. The main selective factor for trap size evolution has been regarded to be the prey size [8,9], hypothesizing that the large traps of *Dionaea* are 'specialized' on capturing large prey and letting too small prey escape because of the meagre nutritional reward. Alternatively, one could hypothesize that the different sizes are determined by the ambient medium in the respective habitat (water versus air). From a mechanical point of view, the effort of realizing a snapping motion against the vicious forces of the ambient water would make smaller traps preferable. This strategy allows aquatic *Aldrovanda* to bear greater than 100 traps per plant and, thus, to increase the capture efficacy. Moreover, the ambient water prevents dehydration and makes structural features, such as several cell layers thick tissues adding to trap thickness, obsolete. This allows for development of a comparably thin structure, limiting *Aldrovanda* to aquatic life and a maximum trap size of 6 mm, which could theoretically be purely hydraulically actuated and, as shown in this study, further speed-boosted by the release of prestress and the kinematic amplification. However, terrestrial *Dionaea* traps are five times larger. To achieve reasonable fast trapping durations in air and to prevent water losses by dehydration, thicker structures and snap-buckling are required. In this context, a detailed investigation of fluid displacement during closure between the two species is of high interest and worth further research. This has been stated in [4], where we show that *Dionaea* traps also function under water, and therefore, prove that the viscosity of the surrounding medium (air versus water) seems not to be the main constraint for the evolution of the different types of snap-trap actuation found in *Aldrovanda* and *Dionaea*.

Data accessibility. The datasets supporting this article have been uploaded as the electronic supplementary material.

Authors' contributions. All authors contributed to the conception and design, analyses and interpretation of data, drafting or revising the article; A.S.W. and P.V. contributed to the acquisition and processing of biomechanical and functional-morphological data, R.S. contributed by generation of FE models.

Competing interests. We declare we have no competing interests.

Funding. This work has been funded by the German Research Foundation (DFG) as part of the Transregional Collaborative Research Centre CRC/Transregio) 141 'Biological Design and Integrative Structures'/project no. A04 (CRC TRR 141 A04). This study was partly supported by the Czech long-term research development (project no. RVO 67985939) for L.A. S.P. acknowledges funding by the Joint Research Network on Advanced Materials and Systems (JONAS).

Acknowledgements. The authors thank Sandra Caliaro for help in thin-sectioning and Dirk Rohleder for kindly nursing the plants.

References

1. Poppinga S, Masselter T, Speck T. 2013 Faster than their prey. New insights into the rapid movements of active carnivorous plants traps. *Bioessays* **35**, 649–657. (doi:10.1002/bies.201200175)
2. Cameron KM, Wurdack KJ, Jobson RW. 2002 Molecular evidence for the common origin of snap-traps among carnivorous plants. *Am. J. Bot.* **89**, 1503–1509. (doi:10.3732/ajb.89.9.1503)
3. Forterre Y, Skotheim JM, Dumais J, Mahadevan L. 2005 How the Venus flytrap snaps. *Nature* **433**, 421–425. (doi:10.1038/nature03185)
4. Poppinga S, Kampowski T, Metzger A, Speck O, Speck T. 2016 Comparative kinematical analyses of Venus flytrap (*Dionaea muscipula*) snap traps. *Beilstein J. Nanotechnol.* **7**, 664–674. (doi:10.3762/bjnano.7.59)
5. Ashida J. 1934 Studies on the leaf movement of *Aldrovanda vesiculosa* L. *Mem. Coll. Sci. Univ. Kyoto Ser. B* **9**, 141–244.
6. Poppinga S, Joyeux M. 2011 Different mechanics of snap-trapping in the two closely related carnivorous plants *Dionaea muscipula* and *Aldrovanda vesiculosa*. *Phys. Rev. E.* **84**, 41928. (doi:10.1103/PhysRevE.84.041928)
7. Iijima T, Sibaoka T. 1983 Movements of K^+ during shutting and opening of the trap-lobes in *Aldrovanda vesiculosa*. *Plant Cell. Physiol.* **24**, 51–60. (doi:10.1093/oxfordjournals.pcp.a076513)
8. Gibson TC, Waller DM. 2009 Evolving Darwin's 'most wonderful' plant. Ecological steps to a snap-trap. *New Phytol.* **183**, 575–587. (doi:10.1111/j.1469-8137.2009.02935.x)
9. Lehtinen S. 2018 Understanding the Venus flytrap through mathematical modelling. *J. Theor. Biol.* **444**, 1–10. (doi.org/10.1016/j.jtbi.2018.02.003)
10. Skotheim JM, Mahadevan L. 2005 Physical limits and design principles for plant and fungal movements. *Science* **308**, 1308–1310. (doi:10.1126/science.1107976)
11. Adamec L. 1997 How to grow *Aldrovanda vesiculosa* outdoors. *Carniv. Plant Newsl.* **26**, 85–88.
12. Adamec L. 1999 The biology and cultivation of red Australian *Aldrovanda vesiculosa*. *Carniv. Plant Newsl.* **28**, 128–132.
13. Elansary HOM, Adamec L, Štorchová H. 2010 Uniformity of organellar DNA in *Aldrovanda vesiculosa*, an endangered aquatic carnivorous species, distributed across four continents. *Aquat. Bot.* **92**, 214–220. (doi:10.1016/j.aquabot.2009.12.002)

14. Adamec L, Kovářová M. 2006 Field growth characteristics of two aquatic carnivorous plants, *Aldrovanda vesiculosa* and *Utricularia australis*. *Folia Geobot.* **41**, 395–406. (doi:10.1007/BF02806556)
15. Schindelin J *et al.* 2012 Fiji. An open-source platform for biological-image analysis. *Nat. Methods* **9**, 676–682. (doi:10.1038/nmeth.2019)
16. R Development Core Team. 2014 *R: a language and environment for statistical computing*. Vienna, Austria: R Foundation for Statistical Computing.
17. Neinhuis C, Edelmann HG. 1996 Methanol as a rapid fixative for the investigation of plant surfaces by SEM. *J. Microsc.* **184**, 14–16. (doi:10.1046/j.1365-2818.1996.d01-110.x)
18. Gibson LJ. 2012 The hierarchical structure and mechanics of plant materials. *J. R. Soc. Interface* **9**, 2749–2766. (doi:10.1098/rsif.2012.0341)
19. Szymanski DB, Cosgrove DJ. 2009 Dynamic coordination of cytoskeletal and cell wall systems during plant cell morphogenesis. *Curr. Biol.* **19**, R800–R811. (doi:10.1016/j.cub.2009.07.056)
20. Colombani M, Forterre Y. 2011 Biomechanics of rapid movements in plants. Poroelastic measurements at the cell scale. *Comput. Methods Biomech. Biomed. Eng.* **14**, 115–117. (doi:10.1080/10255842.2011.593757)
21. Poppinga S, Zollfrank C, Prucker O, Rühe J, Menges A, Cheng T, Speck T. 2017 Toward a new generation of smart biomimetic actuators for architecture. *Adv. Mater.* 1703653. (doi:10.1002/adma.201703653)